International Journal of Sciences: Basic and Applied Research (IJSBAR)

ISSN 2307-4531
(Print & Online)

http://gssrr.org/index.php?journal=JournalOfBasicAndApplied

---

# Monitoring Pollutant Emission with QC Laser Based Mid IR Sensors

Ferdinand Shimei. I. [a*], Chineke, T. C. [b], Nwofor, O. K. [c], Ewurum, B. B. [d]

[a,b,c,d] *Department of Physics and Industrial Physics, Imo State University, P.M.B 2000 Owerri, Nigeria*

[a] *Email: jehos_haphat@yahoo.com*

**Abstract**

Current progress in Mid-IR semiconductor laser technology established on inter-sub-band changed like quantum wells assure a remarkable impact on tunable diode laser-based sensors for trace gases. This paper presents improvement toward the awareness of room-temperature laser-based sensors for combustion-generated pollutants like $NO_2$ and $SO_2$. Laboratory measurements of $SO_2$ at 8.5 µm are presented with detection range on the order of 1 ppm. Further approaches for higher sensitivity measurements in exhaust gas conditions are illustrated, as well as measurements of $SO_x$.

***Keywords***: Pollutant- Combustion- Sensors; Quantum –Cascade; Diode- Laser.

## 1. Introduction

Contemporary jet aircraft engines generate oxidized sulfur type, such as $SO_2$, $SO_3$, and $H_2SO_4$, which may contribute to the formation of aerosols and clouds in the atmosphere [1]. The reaction mechanisms and rates for conversion of combustion-generated $SO_2$ to $SO_3$ and next to $H_2SO_4$ in jet aircraft exhausts are the subjects of severe inspection in the assessment of the atmospheric effects of aviation, which can be determined by quantitative determinations of $SO_2$ and $SO_3$ yields in the exhaust streams of test engines at high-altitude speed atmosphere. Fuel-bound sulfur is currently in jet fuels as pollution and as lubricant agents. For the period of the combustion process in the engine, this sulfur is fundamentally completely corroded to structure $SO_2$, which is exhausted into the atmosphere.

---

* Corresponding author

Some of the $SO_2$ further corroded over a long time scale by atmospheric order to form $H_2SO_4$, which condenses to form tiny aerosol particles. Furthermore, some of the $SO_2$ is rapidly corroded in combustor exhaust stream to generate $SO_3$, which is in turn rapidly transformed into $H_2SO_4$ through result with $H_2O$ in the exhaust. However, [2, 3] elaborated further how $H_2SO_4$ formed in the exhaust stream may deposit on combustion-generated soot particles to produce hydrophilic condensation nuclei, thereby promoting formation of contrails and unrelenting cirrus clouds in the stir of the aircraft. These clouds and their development in highly traveled aircraft passageway can have significant impacts on the radiate heat and chill budgets in the local upper troposphere and lower stratosphere, with extremely uncertain effects on area climate and on mass shift across the tropopause [1]. Thus aircraft-generated high-altitude clouds, resulting from SOx chemistry in the exhaust, may affect global climate and stratospheric ozone dynamics.

Due to potentially severe long-term atmospheric effects, governments and industrial research and development of complex gas turbine engine model are pursuing means of confirming and quantifying the linkages between fuel-bound sulfur, combustion-generated $SO_2$, $SO_3$, and $H_2SO_4$, and the formation of condensation nuclei. Key factor of this research and development is the determination of the kinetics, concentrations, and chemical fates of $SO_2$ and $SO_3$ in combustor exhaust streams. It call for highly sensitive (ppmv level) and quantitative detection of $SO_2$ and $SO_3$ at high temperatures (2800 to 6990 K), reduced pressures (0.2 to 0.4 atm), and elevated $H_2O$ and $CO_2$ mole fractions (0.10 to 0.15) characteristic of combustor exhaust conditions. Summary of the temperature and pressure account through the exhaust turbine and the resultant equilibrium SOx concentration account is shown in Figure 1. Note that thermodynamic equilibrium favors $SO_3$ structure; however it is well recognized that almost all of the emitted sulfur is in the form of $SO_2$ due to the slow kinetic rate of conversion of $SO_2$ to $SO_3$ under these circumstances

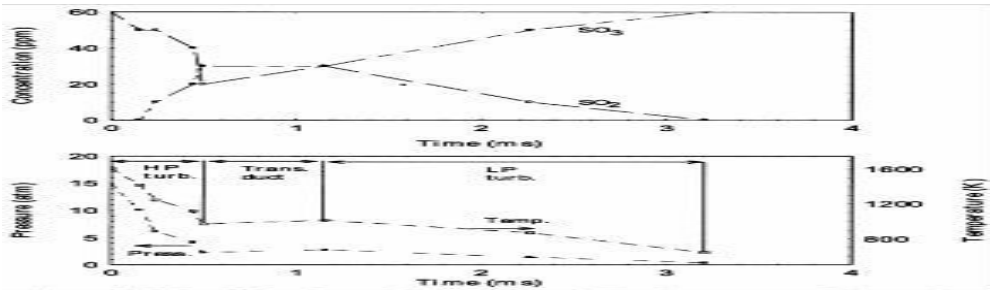


**Figure 1:** shows the calculated equilibrium $SO_2$ from a P-T cycles analysis of a commercial service jet aircraft engine operating with Jet – A fuel having 0.5% sulfur contents and at an overall equivalence ratio of 0.37.(Courtesy Dr. Quang-Viet Nguyen NASA/GRC, May 2000)

### *1.1 Definition of Problem*

The increase in anthropogenic activities from jet aircraft exhaust increased the level of pollution in atmosphere as particulate matter were ejected into the atmosphere in form of fumes from the exhaust of jet aircraft engine through the exhaust. This study intends to assess room-temperature laser-based sensors for combustion-generated pollutants such as NOx and SOx.

### *1.2 Objectives of Study*

The purpose of this study is to identify and quantifying the linkages between fuel-bound sulfur, combustion-generated $SO_2$, $SO_3$, and $H_2SO_4$, and the formation of condensation nuclei.

### *1.3 Significance of the Study*

This study if properly carried out will

- Provide insight to the pollution level in atmosphere.
- Create public awareness and information to the dangers caused by pollution jet aircraft engines.
- Create better quality life and public safety health for the people if air quality of the environment is monitored.
- Reduce sickness arising from short and long term exposure to air pollution.

### *1.4 Limitation of Study*

The limitations of this study include the following: (a) the complexity in ascertaining exact rates for conversion of combustion-generated $SO_2$ to $SO_3$ and next to $H_2SO_4$ in jet aircraft exhaust.

## 2. Review of Related Literature

### *2.1 $SO_x$ Monitoring Techniques*

Although procedure to detect these species have been formulated in several research laboratories, their implementation requires considerable exertion and specialized dexterity in physical chemistry, optics, and spectroscopy, so these methods are not readily available to the combustion engineering community. We observed that investigating the kinetics of $SO_2$ and $SO_3$ has devised means of detecting these species using electronic evolution in the ultraviolet area of the spectrum [4]. $SO_2$ can be detected by absorption or laser-induced fluorescence in its electronic bands near 298 nm. Furthermore, $SO_3$ has absorption bands in the vacuum ultraviolet (145 to 160 nm), and has been detected by laser photo dissociation to excite fluorescence from excited $SO_2$ near 298 nm. Detection of $SO_3$ by this method requires a fluorine excimer laser at about 157 nm, and is unworkable in systems containing substantial concentrations of oxygen since $O_2$ absorbs strongly at the wavelengths required to photo dissociate the $SO_3$. The $SO_2$ electronic band is accessible to pulsed tunable dye lasers, and can also be reached by frequency summing of two high-power near-IR solid state lasers in a non-linear optical crystal.

Infrared fraction of the spectrum present an alternative approach for probing trace-level gas-phase species, mostly by laser absorption in fundamental and overtone vibration-rotation bands. Nevertheless, the infrared absorption approach has in history found less application at high sensitivities than ultraviolet method owing to inherent sensitivity limitations of conventional absorption measurements and to the rareness of tolerable infrared light sources.

More than 15 years, semiconductor laser absorption spectrometers with the utmost sensitivities have operated primarily in the mid-infrared, where the fundamental vibration evolution occurs. These evolutions have the largest infrared evolution strengths for a given molecule, while they arise from single-quantum change in the vibration quantum number. Accordingly they accessed this wavelength region, laser absorption spectrometers have been developed using lead salt diode lasers [5]. Although these devices have achieved high sensitivities and have operated on airplanes, balloons, and combustion facilities, there are several aspects of lead salt lasers that result in a complex instrument design or inhibit routine use. Lead salt lasers are hygroscopic, are highly sensitive to electrostatic discharge, exhibit performance degradation due to temperature cycling, and produce relatively low output power (0.1 to 1 mW). Remarkably, these lasers do not operate at room temperature but require cryogenic cooling. In addition, these lasers are only available in Fabry-Perot designs, with the result that they operate multimode and can require a monochromator to select a single longitudinal mode. They are available in few wavelengths from limited purveyor because of low demand. They found their best use in highly specialized, deep research applications.

### *2.2 Quantum Cascade Lasers*

However, recent development of quantum cascade lasers enables the following major progression in trace type detection: entrance to the strong, mid-infrared fundamental vibration-rotation evolution with a room temperature, single-mode, tunable diode laser [6, 7]. QC lasers realize gain via the transitions of electrons between two sub bands in the conduction band of a coupled quantum well structure. Inversion is created by engineering the lifetimes of the states concerned. The paired electron-injection and active-well regions are replicated many times over (cascaded) to increase output power. Since the evolution occur completely within the conduction band of the material, the output wavelength is determined by the thickness of the active region and is independent of the band gap. QC lasers can be fabricated at any wavelength from ~ 4.6 to 17 μm using AlInAs/InGaAs lattices. The QC laser design overcomes two main drawbacks of lead salt diode lasers. First, they can be operated at room temperature, and second, depressed response (DRP) versions can be fabricated to operate on a single longitudinal mode. By accessing the stronger bands in the mid-infrared fingerprint region, a QC laser absorption spectrometer requires a considerably shorter path than a near-IR device of comparable sensitivity. These advantages result in an overall sensor system that will be smaller and less complex than existing lead salt or near-IR sensors. Thus, the advent of QC lasers enables a new generation of laser-based sensors which achieve the sensitivities of lead salt laser sensors and incorporate the robustness and ease of operation of near-IR diode laser sensors.

Many groups have recently delivered applications of QC lasers to trace gas sensing [8]. Sensitive absorption spectroscopy using frequency modulation (FM) detection and a room temperature, pulsed (DRP) QC laser has been reported. Receptive absorption spectroscopy has also been demonstrated with cryogenically cooled, as [9]. The continue wave (cw) QC lasers using either FM detection or photo acoustic detection techniques [10]. Detection of isotopic composition has also been demonstrated using cryogenically cooled cw QC lasers [11].

However, works has focused on quasi-cw, room temperature operation of the laser source with high sensitivity detection achieved using the balanced ratio metric technique [12].

They established the operation of a breadboard QC laser system to detect $N_2O$ and NO near 5.4 μm, and are currently developing a field sensor for measurements of formaldehyde in the troposphere. Their general approach is to combine QC laser light sources with multipass absorption cell and noise reduction techniques formerly developed for our near-IR diode laser sensors, to achieve sub-ppmv sensitivities for infrared-active species. While QC lasers can be operated cw at cryogenic conditions, they took the approach of pulsed operation at thermoelectrically cooled conditions near room temperature. The noise reduction techniques include [13]:

- Reduction of thermal noise through use of liquid-nitrogen-cooled field of view.
- Dual-beam, unbiased share metric detection (USD). The USD system is an analog circuit which ratios the signal and reference beams to cancel common mode laser intensity fluctuations. Here the USD is interfaced with the pulsed laser source by operating the USD circuit at a bandwidth which is low adequate to standard the laser pulses into a "quasi-cw" sign, but high sufficient to reject common mode laser noise.

## 3. Methodology

### *3.1 IR Spectroscopy of $SO_2$ and $SO_3$*

We examined the quantitative infrared spectroscopy of $SO_2$ and $SO_3$ via data bases existing in the literature. A detailed, line-by-line compilation of the vibration-rotation transitions of $SO_2$ is given in the HITRAN96 data base on atmospheric infrared transitions. The HITRAN cipher and data base was urbanized by the Air Force Research Laboratory to provide model simulation capability for high-resolution infrared absorption spectra of atmospheric species as functions of temperature, pressure, concentration, and path length. We also performed spectral modeling simulations using the commercial version of HITRAN marketed by Ontar Corp. The modeling calculations simulated the conditions of our room-temperature FTIR and QC laser measurements, as well as the conditions of high-temperature combustor exhaust measurements at both atmospheric and reduced pressures. The high-temperature calculations also included simulations of the absorption spectra of $H_2O$ and $CO_2$, which are the most important sources of spectral interference with $SO_2$ and $SO_3$ detection in combustor exhaust streams. The high-temperature simulations of $H_2O$ and $CO_2$ absorption spectra used the HITEMP spectroscopic data base for these species; this data base includes hot-band transitions which are applicable to high-temperature systems up to ~ 1000 K. Unfortunately, there is no high-temperature analogue of this data base for $SO_2$, so the scaling of $SO_2$ transitions and line strengths to combustor exhaust temperatures is not well validated.

The experimental $SO_2$ spectra were obtained at room temperature with a commercial FTIR spectrometer (Midac Corp.) interfaced to a multipass absorption cell. The cell was connected to a gas supply manifold and a vacuum system allowing operation from vacuum to 1 atm. The multipass optical system within the cell was set up to give 20 passes, resulting in a total path length of 4.90 m. Matched pairs of background (cell evacuated) and sample (cell containing gas sample) spectra -1 were obtained at 0.5 cm spectral resolution by co-adding 33 interferograms for each case.

The background and sample: (a) Spectra were ratio to give quantitative spectra of absorbance, in (Io/I), versus evolution frequency in cm. (b) The measurements were performed over the pressure range 0.1 to 0.4 atm for a commercial gas mixture of 502.5 ppmv $SO_2$ diluted in $N_2$.

As demonstrated by the experimental spectra in Figure2: shows $SO_2$ has two vibration bands in the 6 to 9 µm region: (a) the strong asymmetric stretch (υ3) band centered near 1359 cm (7.35 µm).

(b) The weaker symmetric stretch band (υ1) centered near -1050 cm (8.7 µm).

The 8.6 µm QC laser measurements carried out for this exertion probe the latter, υ1 band; though, evolution in the υ3 band will achieve the highest possible sensitivity. The most recently reported integrated band intensities at 295 K (including hot band contributions) are 0.39 x $10^{-17}$ and 2.98 x $10^{-17}$ cm/ (molecule $cm^{-2}$) for the υ1 and υ3 bands, respectively.

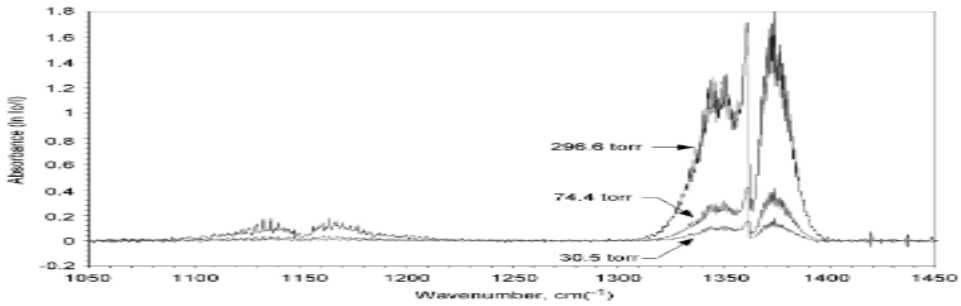


**Figure 2:** FTIR spectra of 502 ppm $SO_2$, balance $N_2$ at 295 K in a 4.89m path (Courtesy atmos.)

Figure 3 shows the result absorbance spectrum to check for spectral interferences by air at room temperature, we filled the FTIR absorption cell to atmospheric pressure with room air at ~ 20% relative humidity, overlain with the $SO_2$ spectrum. All the evolutions in the room air spectrum are due to $H_2O$, as confirmed by HITRAN calculations. At room temperature, there are no interfering $H_2O$ transitions in the $SO_2$ (υ1) band, confirming that the laboratory QC laser measurements at 8.5 µm did not require a purge flow in the beam path. Though, there are several $H_2O$ features in the region of the $SO_2$ (υ3) band, as this region is near the edge of the strong $H_2O$ (υ2) band centered near 6.2 µm. $H_2O$ interference in this region is a key factor in the design of a system for high-temperature measurements, as described below.

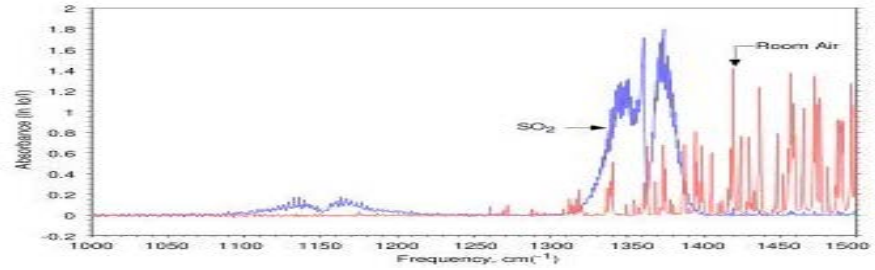


**Figure 3:** Comparison of FTIR spectra of $SO_2$ and room air, showing spectral overlap of $H_2O$ absorption features (Courtesy Atmos.).

The infrared spectrum of gas-phase $SO_3$ consists of a υ3 band centered at 1392.3 cm (7.19 μm), and υ2 and υ4 bending bands near 500 cm (20 μm) [14, 15]. $SO_3$ is a planar symmetric (D3h) molecule, and thus the symmetric stretch υ1 is infrared-inactive. Only the υ3 band is accessible to a QC laser. Full spectroscopic measurements of this band have been reported by Henfrey and Thrush. A section of their published spectrum, obtained at 0.01 $cm^{-1}$ resolution for 10 Torr of $SO_3$ in a 15 cm gas cell, is shown in Figure 4. The authors report detailed spectroscopic constants which can be used to calculate the line-by-line transition frequencies; though no line strength data are available. The peak absorbencies shown in Figure 4 are consistent with line strengths similar in magnitude to those for $SO_2$ (υ3). A broad computer literature search indicates that there are no open-literature data on the line power or high-temperature spectroscopy of this band.

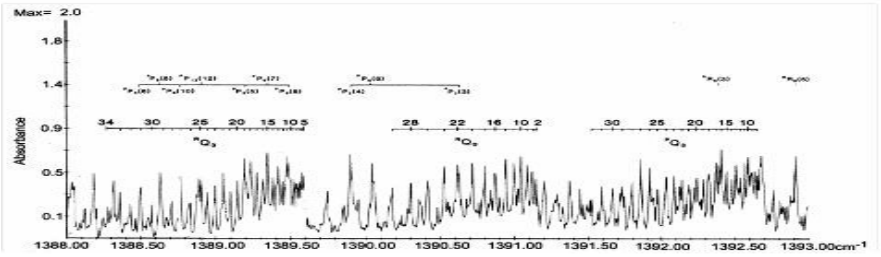


**Figure 4:** High resolution spectrum of the center of the $SO_3$ ($v_3$) band (Courtesy Atmos.).

## 4. Data Analysis

### *4.1 Laser Measurements on Quantum Cascade*

Mutually dispersed response (DRP) and non-dispersed response (DRP) Quantum Cascade (QC) laser devices working near 8.5 μm were available to support this exertion. The dispersed response lasers of carrier D2307CC2 were partially characterized at Lucent for pulsed operation near room temperature. Figure5: is a plot of the temperature tuning for two representative QC lasers. This data was obtained for pulsed operation at 82.8 kHz with 60 ns pulse width.

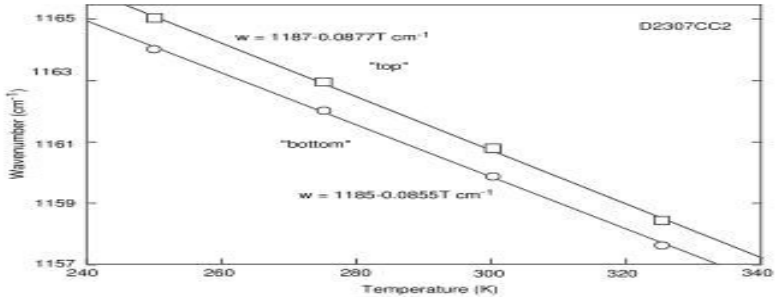


**Figure 5:** show Example of QC laser temperature tuning data for two devices (top and bottom) (Courtesy Atmos.)

The current tuning rate is approximately $10^{-2}$ $cm^{-1}$/mA (300 MHz/mA). Figure6: shows L-I and V-I curves presented for the laser.

These QC lasers have a current threshold of approximately 2.6 to 3.6 near room temperature and have a distinctive emission roll-off at higher currents. In between, the L-I curve is linear.

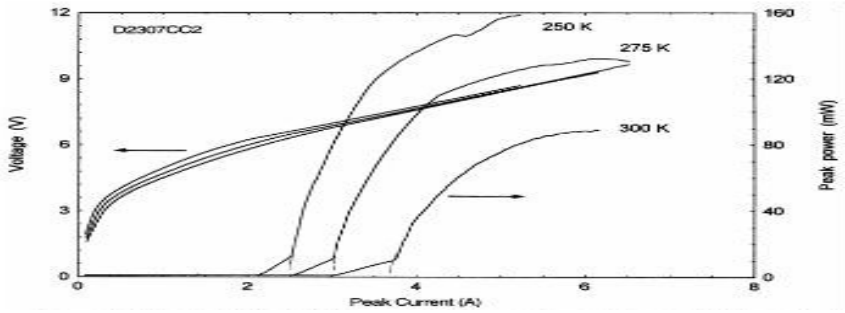


**Figure 6:** shows example L-1 and V-I curve for the same two devices as in figure.5. (Courtesy Atoms)

These procedures require a reasonably high compliance voltage (~5 V) compare to other semiconductor diode lasers. For zero bias, the devices have an efficient resistance of about 21 ohm, which decreases to 1.5 ohm above threshold. They described the laser system and drive current configuration for these experiments [12]. Absorption dimension were classically made by pumping the laser with a 5 kHz injection current pulse train consisting of 66 ns pulses for an overall duty cycle of 0.03%. The waveform be superimposed ahead a low-amplitude slope waveform with a typical repetition frequency of 100 Hz.

The collimated laser beam exits the mount and it split into a signal and a reference beam using an ar-coated Ge beam splitter. The signal beam propagates through a 0.5 m electro polished, stainless steel absorption cell having ar-coated, 30' wedged Ge windows. After exiting the cell, the beam is refocusing onto an LN2-cooled photovoltaic HgCdTe detector by a 1 in. diameter, ar-coated Ge f/1 lens. Similarly, the reference beam is refocused onto a second HgCdTe detector using another Ge lens. Rider was made to purge the beam paths. The detectors were 1 mm diameter devices. Each detector was fitted with a 61 deg cold field-of-view. This helps minimize the background current arising from collection of ambient radiation.

Outputs from the detectors were sent to a high gain current preamplifier then into gated integrators. The gated integrator signals were sampled, recorded and integrated to produce a real time history of the number density of the type under analysis. This dual beam, predictable detection technique allowed us to investigate spectral absorbance down to ~0.5%.

We observed the compound absorption aspect that arises from the partial overlie of six lines of the υ1 band that occur near 1160.76 cm (8.63 μm). These evolutions are listed in Table 1.

A forecasted absorption spectrum near 1159 cm, for 100 ppmv of $SO_2$ at 100 Torr, is shown in Figure 7. Further modeling with HITRAN96 at lower pressures specify that strong absorption spectra of individual transitions can be produced in the Doppler-broadened limit, using 1 to 10 Torr of undiluted $SO_2$ over the available 0.5 m path.

**Table 1:** Entity evolution in v1 Band of $SO_2$ causative to the Observed Absorption Features

| Frequency ($cm^{-1}$) | Line Strength ($cm^{-1}$(molecle$^{x}$$cm^{-2}$) | $Z_1$ | $Z_2$ |
|---|---|---|---|
| 1161.49479 | 1.53 x $10^{-21}$ | 8 3 6 | 6 2 6 |
| 1161. 70377 | 3.40 x $10^{-21}$ | 25 5 21 | **25 2 20** |
| 1161. 77537 | 5.21 x $10^{-21}$ | 16 2 16 | **15 1 15** |
| 1161. 77313 | 5.38 x $10^{-21}$ | 15 1 15 | 16 0 16 |
| 1161. 79491 | 3.22 x $10^{-21}$ | 17 2 16 | 16 2 17 |
| 1161. 81365 | 2.89 x $10^{-21}$ | 18 2 17 | 17 1 16 |

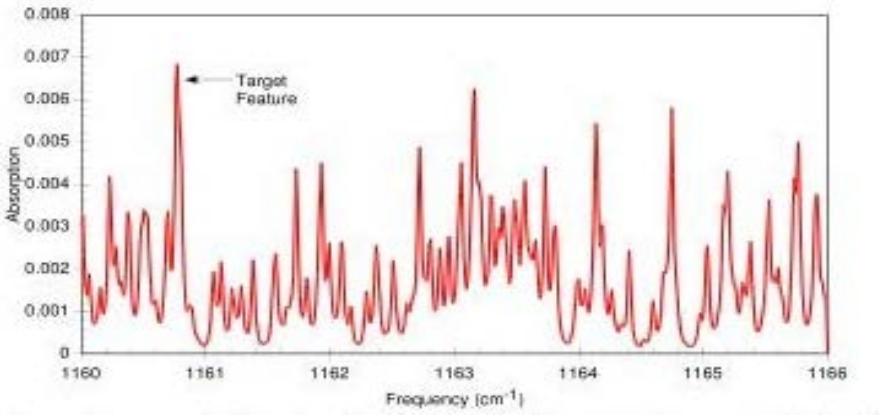


**Figure 7:** Computed spectrum of $SO_2$ absorption features near 1160 $cm^{-1}$, for 100ppm, $SO_2$/air at 100 Torr. (Courtesy Atmos.)

Certainly is important to note that the band spectrum for $SO_2$ is highly crammed and overlapped, even under low pressure, Doppler-broadened conditions. However, we do not sample a true zero-absorption baseline, rather the differential absorption produced by the compound, overlie features.

Model experimental absorption spectrum is existing in Figure 8. This spectrum was obtained for 0.5 Torr 16 -2 (1.6 x 10$cm^{-3}$) of $SO_2$ at 296 K, and is an average of ten single sweeps (0.1 s average). The thinner line is a running average of ten data points and advances the signal-to-noise ratio.

The peak absorption is 0.07 and the signal-to-noise ratio (SNR) is ≈30, which entail minimum detectable peak absorption of 3 x $10^{-3}$ for 2.6 x $10^{14}$ $cm^{-3}$ $SO_2$ and a 1 m path. By extrapolating these results to the typical detection limits of dispersed response or FM-based spectrometers and accounting for increased collision broadening near atmospheric pressure, we approximate detection sensitivity at room temperature of about 0.1ppm

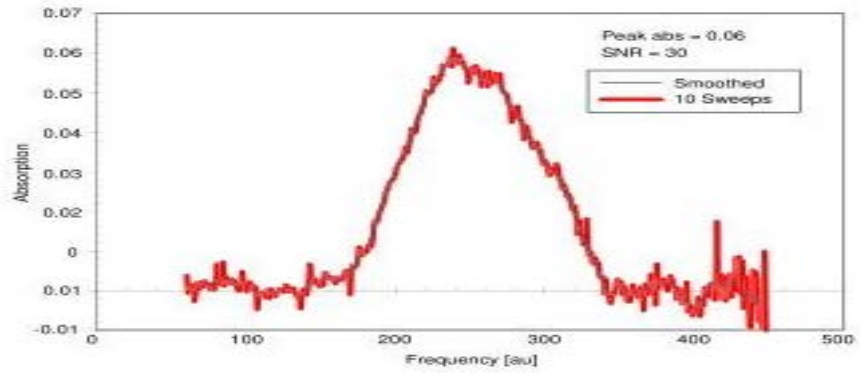


**Figure 8:** Examples QC laser absorption spectrum of the compound $SO_2$ feature near 1160.75$cm^{-1}$.The spectrum was obtained with 9.5 Torr $SO_2$ at room temperature in a 50cm cell. (Courtesy Atmos.)

### *4.2 Exhaust Gas Simulation Measurements*

The annex of the present room-temperature results will require QC lasers working at different wavelengths so as to optimize the sensitivity of the beleaguered lines as well as ensure that they are free from interference by major exhaust gas type such as $CO_2$ and $H_2O$. In order to determine best wavelengths for $SO_2$ and $SO_3$, we used broad spectral simulations by HITRAN and HITEMP to forecast high-resolution spectral absorbance for a variety of combustion exhaust situation from 0.1 to 1 atm. A supposed set of environment used here and representative of many exhaust gas conditions in flight are P~ 0.2 atm, T~ 700 K, $\Omega CO_2 \sim 0.1$, and $\Omega H_2O \sim 0.1$.

The forecasted spectra were estimated in terms of absorbance per meter of path length for 1 ppmv of $SO_2$. In calculating the detection limits in terms of concentration and path length, we assumed a minimum detectable absorbance of 1 x $10^{-5}$. They discussed this projected value based on our breadboard QC laser measurements at 5.5 and 8.5 µm with and without the DRP noise- canceling circuit [12]. The absorbance computations used Beer' and thus neglected the possible laser line broadening effects due to thermal frequency chirp [12]. The computation also used the pressure broadening coefficient for $SO_2$ in air contained in the HITRAN data base and thus neglects possible additional broadening due to collisions with $H_2O$ and $CO_2$. Despite these limitations, the HITRAN and HITEMP spectral modeling computations provide the best estimates within the known state of the art for high-temperature, high-resolution infrared absorption by $SO_2$, $H_2O$, and $CO_2$.

However, the absorbance spectra for $SO_2$ ($\upsilon 3$), $H_2O$, and $CO_2$ in the 1321 to 1390 cm region (7.3 to 7.5 µm), for P = 1 atm, T = 700 K, $\Omega H_2O = 0.2$, $\Omega CO_2 = 0.1$, $\Omega SO_2 = 1$ ppmv, were simulated [1]. The $SO_2$ absorbencies generally exceed those of $CO_2$, and are well above the estimated absorbance detection limit of $\approx 10^{-5}$. Though, they are much lower than those of $H_2O$. Most significantly, at 1 atm the pressure-broadened wings of the $H_2O$ transitions fill in the gaps between the evolutions, so that the $H_2O$ absorbance is near-continuum which is always at least 100 times greater than that of $SO_2$ at 1 ppmv. Higher resolution simulations of selected gap in the $H_2O$ spectrum indicate that spectral discrimination of $SO_2$ features under these conditions would be extremely difficult, and would require refined data processing and spectral fitting procedures to identify 10 to 100 ppmv of $SO_2$.

In distinction, there is a lot less $H_2O$ interference in the υ1 band, as shown in Figure 9 for the same 1 atm conditions. This is steady with our experimental observations at room temperature. Though the $SO_2$ absorbencies for 1 ppmv-m are near the probable detection limit of ~ $10^{-5}$, the features of $SO_2$ are much easier to distinguish from the $H_2O$ background in the spectral windows.

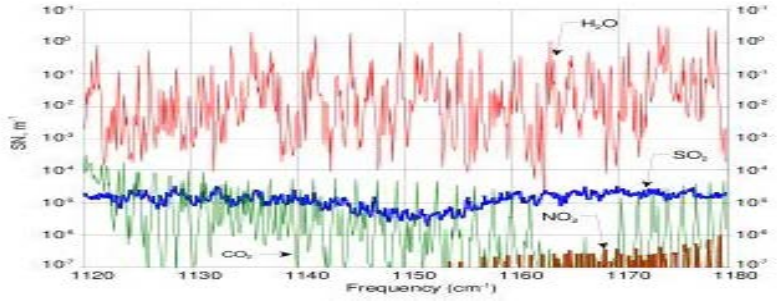


**Figure 9:** Computed atmospheric pressure exhaust gas absorption spectra near $SO_2$ (v1) band

Therefore at 1 atm and elevated temperature, $SO_2$ is probable to be further simply detected in the weaker υ1 band than in the υ3 band. Pro υ3 band evolution at reduced pressure; the peak $SO_2$ absorbance for 1 ppmv-m is abridged, however yet surpass $10^{-5}$. More importantly, the collision-broadened wings of the $H_2O$ lines are seriously diminished, opening several spectral windows where $SO_2$ skin can be known. As abridged pressure conditions are more relevant to engine exit conditions at altitude, we focus on those conditions for more detailed computation in the $SO_2$ (υ3) band.

To reproduce the conditions of engine exhaust measurements at high-altitude cruise conditions, we carry out a series of high-resolution calculations throughout the 1321 to 1390 cm region for P = 0.2 atm, T = 700 K, $\Omega H_2O$ = 0.1, $\Omega CO_2$ = 0.1, $\Omega SO_2$ = 1 ppmv. These calculations led to the recognition of three suitable spectral regions for detection of $SO_2$. These are illustrated in Figures 10 through 12. Here we show the entity contributions from $H_2O$, $CO_2$, and $SO_2$, and the sum of the three. In each of these spectral windows, a scan of the laser frequency will give quantitative identification of $H_2O$ and $SO_2$; in addition, spectral scans near 1342 cm will give $CO_2$ determination as well. Gradual determinations of $SO_2$ along with $H_2O$ and or $CO_2$ will allow direct determination of the emission index of $SO_2$ with a single sensor. The 1333 $cm^{-1}$ region offers the strongest $SO_2$ evolution however the 1342 $cm^{-1}$ region has better isolation of the $SO_2$ lines. The forecasted $SO_2$ crest absorbance in these windows for 1 ppmv-m are moderately above the probable detection limit of ~ $10^{-5}$, which shows that sub-ppmv levels of $SO_2$ will probably be visible with a ≈ 1 m path length.

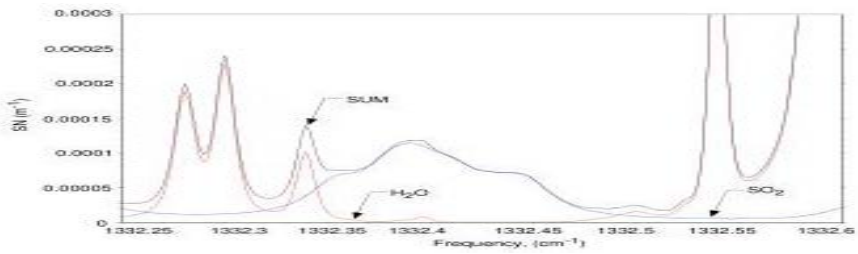


**Figure 10:** Computed exhaust gas spectra at 0.2 atm near 1332$cm^{-1}$ (Courtesy Atmos.)

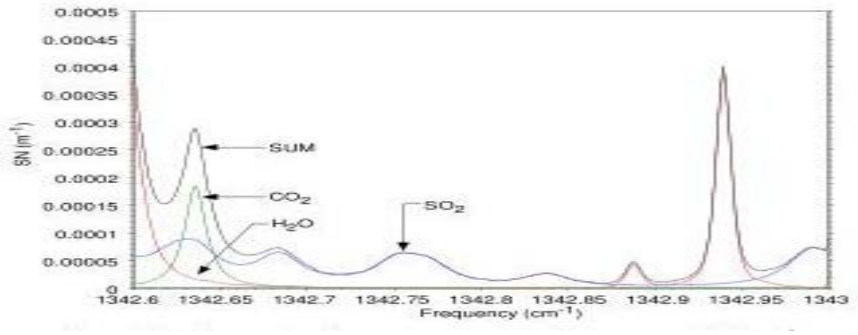


**Figure 11:** Computed exhaust gas spectra at 0.2 atm near 1343 $cm^{-1}$ (Courtesy Atmos.)

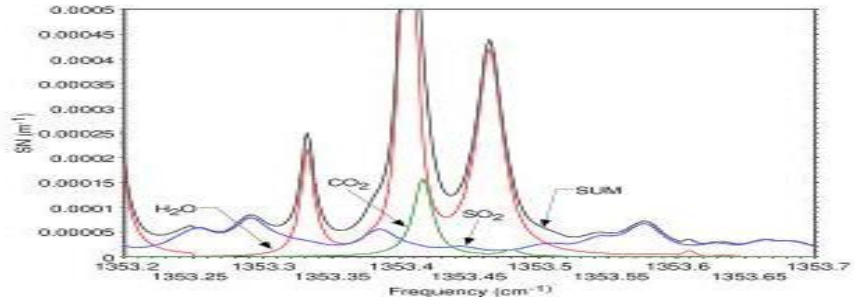


**Figure 12:** Computed exhaust gas spectra at 0.2 atm near 1354 $cm^{-1}$ (Courtesy Atmos.)

Spectral model of the $H_2O$ and $CO_2$ absorbance near the $SO_3$ band center are shown in Figure 13 for the 0.2 atm exhaust conditions. The $H_2O$ baseline absorbance is fairly higher in this region, (2 to 4) x $10^{-4}$. Depended on the peak absorbance of $SO_3$ at room temperature for this region, we estimate peak $SO_3$ absorbance for 1 ppmv-m to be about 8 x $10^{-5}$ as indicated by the bar on the graph.

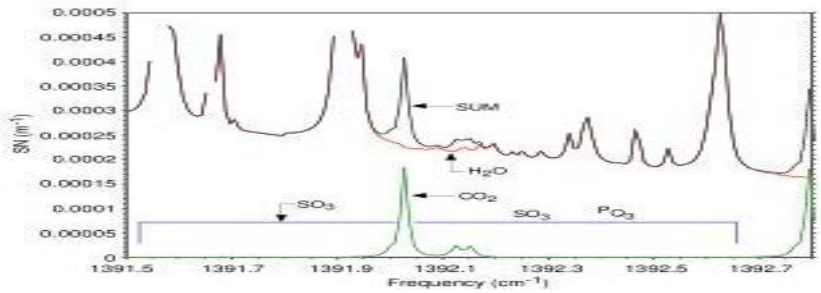


**Figure 13:** Computed exhaust gas spectra at 0.2 atm near 1392 $cm^{-1}$ (Courtesy Atmos.)

$SO_3$ structure should be readily detectable among $H_2O$ features near 1391.2 cm. It shows that $SO_3$ can likewise be detected to ~ 1 ppmv or less with a 1 m path length. Like with $SO_2$, it is likely that spectral scans of the laser will permit instantaneous determination of $H_2O$ and/or $CO_2$, therefore docile the emission index of $SO_3$. There may be other spectral casement for detection of $SO_3$, nevertheless the region to lower frequency contains increasing contributions from $SO_2$ ($\upsilon 3$), while the region to higher frequency contains increasing contributions from $H_2O$ ($\upsilon 2$). Decisive determination of the detection casement for $SO_3$ awaits direct spectral measurements at representative temperatures and pressures.

## 5. Conclusion

We used two mixtures of laboratory experimental measurements and spectral modeling calculation to evaluate and quantify the feasibility of high-sensitivity detection of $SO_2$ and $SO_3$ in combustor exhaust streams, using room-temperature quantum cascade laser absorption at precise operating wavelengths near 7 μm. Due to severe interference from collision broadened $H_2O$ lines at 1 atm, it appears that the QC laser absorption method is best suited for the sub atmospheric conditions of high-altitude simulation test facilities when applied to the trace levels found in aircraft emission exhaust streams.

- **Spectral** modeling model of high-resolution infrared absorption spectra for high-altitude test chamber conditions (0.2 atm, 700 K) specify a few discrete spectral casement between 7 and 7.5 μm where $SO_2$ and $SO_3$ absorption features can be observed with minimal interference from $H_2O$ and $CO_2$ in the exhaust stream. Through comparisons of the predicted peak absorbance and the expected detection limit given above, it is likely that both $SO_2$ and $SO_3$ can be detected at or below 1 ppmv, with a path length of 1 m, using a multipass optical system.
- **Laboratory** measurements of QC laser absorption by $SO_2$ at 8.6 μm shows a breadboard QC laser detection system and point to likely detection limits that can be achieved for a fully developed prototype sensor system. Based on straightforward projections of design improvements in laser intensity on detector, pulse generation electronics; heat-sinking of the laser chip, reduction of detector thermal noise, and quasi-cw balanced ratio metric rejection of common mode noise, we conservatively estimate a noise-equivalent absorbance detection limit of approximately $\approx 1 \times 10^{-5}$.

## Acknowledgment

The authors sincerely thank Dr. Quang-Viet Nguyen of NASA for providing exhaust gas composition simulation shown in figure1 and some other figures from the atmospheric journals.

## Reference

[1] Friedl, R.R. Atmospheric Effects of Subsonic Aircraft: Interim Assessment Report of the Advanced Subsonic Technology Program, NASA Reference Publication 1400, 1997.

[2] Wyslouzil, B.E., Carleton, K.L; Sonnenfroh, D.M; Rawlins, W.T; and S. Arnold, Observation of Hydration of Single, Modified Carbon Aerosols, Geophys. Res. Lett. 21, p. 2107, 1994

[3] Rawlins, W.T., Kang, S.G; Sonnenfroh, D.M; Carleton, K.L; and Wyslouzil, B.E; Activation of Carbon Aerosol by Deposition of Sulfuric Acid, Biomass Burning and Global Change, Levine, J.S; Edu MIT Press, Cambridge, MA, 1996, Vol. 1, pp. 540-544.

[4] Suto, M.; Ye, C; Ram, R.S; and Lee, L.C; $SO_2$ Fluorescence from Vacuum Ultraviolet Dissociative Excitation of $SO_3$, J. Phys. Chem. 91, p. 3262, 1987.

[5] Berkoff, T.A; Wormhoudt, J; and Miake-Lye, R.C; Measurement of $SO_2$ and $SO_3$ Using a Tunable Diode Laser System, SPIE Proceedings 3534, p. 686, 1998.

[6] Faist, J., Capasso, F; Sivco, D.L; Sirtori, C; Hutchinson, A.L; and Cho, A.Y; Science 264, p 553, 1994.

[7] Gmachl, C., Faist,J; Baillargeon, J.N; Capasso, F; Sartori, C; Sivco, D.L; et al Complex- Coupled Quantum Cascade Distributed-Feedback Laser, IEEE Photonics Tech. Letts. 9, p. 1090, 1997

[8] Namjou, K; Cai ,S; Whittaker, E.A; Faist, J; Gmachl, C; Capasso, F; et al Sensitive absorption spectroscopy with a room-temperature distributed-feedback quantum- cascade laser, Opt. Letts. 23, pp. 219-221, 1998

[9] Sharpe, S.W; Kelly, J.F; Hartman, J.S; Gmachl, C; Capasso, F; Sivco, D.L; et al High resolution Doppler limited spectroscopy using quantum- cascade distributed-feedback lasers, Opt. Letts. 23, pp. 1396-1398, 1998

[10] Paldus, B.A; Spence, T.G; Zare, R.N; Oomens, J; Harren ,F.J.M; Parker, D.H; et al Photoacoustic spectroscopy using quantum-cascade lasers, Opt. Letts. 24, pp. 178- 180, 1999.

[11] Kosterev, A.A., Curl, R.F; Tittel, F.K; Gmachl, C; Capasso, F; Sivco, D.L; et al Methane concentration and isotopic composition measurements with a mid-infrared quantum-cascade laser, Opt. Letts. 24, pp. 1762-1764, 1999.

[12] Sonnenfroh, D.M., Wetjen, E.W., Miller, M.F., Allen, M.G., Gmachl, C., Capasso, F., et al Mid-IR Gas Sensors Based on Quasi-CW, Room-Temperature Quantum Cascade Lasers, Paper No. 2000- 0641, 38th AIAA Aerospace Sciences Meeting, January, 2000. A revised version, Application of Balanced Detection to Absorption Measurements of Trace Gases with Room-Temperature, Quasi-CW QC Lasers, publication in Applied Optics, September, 2000.

[13] Allen, M.G., Carleton, K.L; Davis, S.J; Kessler, W.J; Otis, C.E; Palombo, D.A; et al Ultra-Sensitive Dual-Beam Absorption and Gain Spectroscopy: Applications for Near-IR and Visible Diode Laser Sensors, Appl. Opt. 34, p. 3240, 1995.

[14] Henfrey, N.S., and Thrush, B.A; The v3 Band of $SO_3$ at High Resolution, Chem. Phys. Lett. 102, p. 135, 1983.

[15] Oritgoso, J. R; Escribano, and A.G. Maki, The v2 v4 IR Bands of SO3, J. Mol Spectrosc. 138, p. 602, 1989.